



NUMERICAL SIMULATION OF PILE PINNING-TYPE LATERAL SPREADING MITIGATION USING XCC AND CIRCULAR PILES

A.W. Stuedlein⁽¹⁾, W. Li⁽²⁾, Y. Chen⁽³⁾, H. Liu⁽⁴⁾, Zhao Cheng⁽⁵⁾

⁽¹⁾ Associate Professor, Oregon State University, armin.stuedlein@oregonstate.edu

⁽²⁾ Assistant Professor, Changshu Institute of Technology, lwwgeo@hotmail.com

⁽³⁾ Professor, Hohai University, ymch@hhu.edu.cn

⁽⁴⁾ Professor, Chongqing University, hliuhhu@163.com

⁽⁵⁾ Senior Geomechanics Engineer, Itasca Consulting Group, Inc., zcheng@itascacg.com

Abstract

The pile-pinning technique for mitigation of liquefaction-induced lateral spreading deformations has been proven to provide an effective means to reduce seismic deformations. This paper summarizes the results of a comprehensive set of 3D numerical simulations aiming to evaluate and compare the performance of circular piles to a novel cast-in-place pile with an X-shaped cross-section, termed the XCC pile. 3D simulations are conducted using the unit cell approach with periodic boundary conditions to evaluate the response of a pile in the center of pile-improved ground. A 3D formulation of the critical-state compatible, stress ratio-controlled Dafalias-Manzari model is used to capture cyclic stress-strain hysteresis and the accumulation of liquefaction-induced lateral displacements. Models without piles and subject to various ground motions are used as the references for the comparisons. Design variables investigated for the pile-improved ground include the cross-section shape, pile spacing, and the slope angle. The performance of the pile-improved ground is evaluated in terms of lateral displacements, and the shear and moment generated with the piles due to soil-pile interaction. The simulations show that the XCC pile-improved ground can effectively reduce lateral spreading-type deformations, and perform better than circular piles sharing the same cross-section area or similar performance to circular piles with the same maximum section dimension, indicating the benefit of its efficient cross-section. Regardless of cross-sections used, the Arias Intensity is shown to be a reliable predictor of pile-pinning performance metrics.

Keywords: numerical modeling; lateral spreading; piles; X-shaped cross-section; lateral spreading mitigation

1. Introduction

Owing to the potential for significant damage arising from liquefaction-induced lateral spreading failure, geotechnical earthquake engineers continue to seek ground improvement alternatives to limit lateral displacements of gently-sloping ground. Common ground improvement alternatives include densification-type improvements (e.g., vibro-compaction[1], dynamic compaction[2], displacement piling[3,4], and sand compaction piles[5]), reinforcement (e.g., jet grouting[6], deep soil mixing[7], vibro-replacement[8]), and drainage[9,10], or some combination of these techniques [3,4,8]. Provided that sufficient rotational stiffness (i.e., fixity) of piles can be achieved within a bearing layer, the pile-pinning method for lateral spreading mitigation has been shown to be promising[11-15]. Related studies, focusing mainly on the structural response of the piling[16-18], reinforce that pile-pinning can serve as an effective mitigation alternative. However, further studies on the soil-pile interaction and lateral displacement of sloping ground are required to establish the amount of mitigation (e.g., pile spacing) necessary to achieve displacements within tolerable limits.

This paper expands previous experiments[13] and 3D numerical studies[19] on circular and novel, X-shaped concrete (XCC) piles deployed to mitigate lateral spreading displacements using the pile-pinning method. The XCC pile (Fig. 1c) presents significant advantages over circular piles, because it provides a greater maximum dimension in cross-section than a circular pile with the same area (or volume per unit length), or smaller volume for a given maximum dimension in the cross-section. The XCC pile is cast-in-place using specialized equipment commonly available in China and is used for both densification-type ground



improvement[21] and support of structures[22-23]. This paper compares the effect of slope inclination angle, pile shape (circular vs. X shape), pile diameter, and pile spacing on the soil response, soil-pile interaction, and lateral displacements of pile-improved sloping ground for a single ground motion record. Thereafter, the response of XCC and circular piles with eight different ground motions are evaluated in terms of Arias Intensity, which is shown to correlate strongly to the maximum residual lateral displacement and the maximum shear force and bending moment induced within the pile in response to strong ground motion. The XCC pile section is shown to offer improved material volume and lateral spreading mitigation performance efficiencies relative to circular, cast-in-place piles.

2. Description of the Numerical Model

2.1 Numerical Mesh and Boundary Conditions

The modeling strategy adopted to evaluate the pile-pinning lateral spreading mitigation of XCC and circular piles using FLAC3D[24] was that of the unit cell to reduce computational demands. Unit cells are commonly implemented to model ground improvements that are applied over a large area using area tributary to a single element, for example with pre-fabricated vertical drains[25,26], stone columns[27-29], and deep soil mixed columns[29]. Furthermore, half of the unit cell may be simulated due to symmetry[29], allowing for additional computational efficiencies. Figure 1 presents the typical finite difference mesh used to simulate XCC and circular piles, within the half-unit cell. Piles are founded within a 1 m thick dense sand deposit (relative density, $D_r = 70\%$) overlain by a 9 m thick deposit of medium dense sand deposit ($D_r = 40\%$). Inclination of the ground surface and corresponding static shear stresses are simulated by decomposing gravitational acceleration into vertical and horizontal components $g \cos\theta$ and $g \sin\theta$, respectively[30]. The boundary conditions include:

1. Periodic boundary conditions in the direction of shaking: the displacements of corresponding nodes at the same elevation on the left and right vertical boundaries are attached in all three directions.
2. Symmetrical boundary conditions perpendicular to the direction of shaking: symmetrical boundary conditions were achieved by rollers (i.e., fixed out-of-plane displacement).
3. Boundary conditions at the base: the base was fixed during static equilibrium and switched to a quiet boundary prior to dynamic analysis to absorb reflected waves to represent a compliant base.
4. Application of ground motions: equivalent shear stress time histories derived from the corresponding acceleration time histories were applied at the model base in the shaking direction.

2.2 Soil and Pile Properties and Constitutive Model Parameters

The medium dense and dense soil deposits are modeled using the stress-ratio controlled, critical state-compatible Dafalias-Manzari (D-M) plasticity model calibrated to the cyclic response of Toyoura sand reported previously[31,32]. The D-M model was implemented in FLAC3D by Cheng et al.[33] and is available at the Itasca User-Defined Model (UDM) website[34]. Table 1 summarizes the model parameters used in this study. One X-shaped (XCC) and two circular, cast-in-place concrete piles are modeled with diameters, D , equal to 0.6 m, 0.48 m and 0.6 m, respectively, by a linear-elastic material with a density of $3,200 \text{ kg/m}^3$. The geometry of the XCC pile, shown in Fig. 1c, is further defined by $b = 0.12 \text{ m}$, and $\alpha = 90^\circ$, representing the typical XCC section. The flexural rigidity of the XCC pile, EI , is $6.0 \times 10^4 \text{ kN m}^2$. The EI for the two circular piles (denoted CA and CD herein) are $5.2 \times 10^4 \text{ kN m}^2$ and $1.3 \times 10^5 \text{ kN m}^2$, respectively. The CA pile, with $D = 0.48 \text{ m}$ shares the same volume of concrete as the XCC pile with $D = 0.6 \text{ m}$, whereas the CD pile shares the same maximum in-plane dimension as the XCC pile. Although the maximum in-plane dimension of the XCC and CD pile are the same (i.e., 0.6 m), the XCC pile requires much less volume of concrete owing to its shape.

The possible flow of liquefied soil around the piles during shaking[11,13] is facilitated using Mohr-Coulomb type interface elements. Interface elements are characterized by their normal and shear stiffness, friction and dilation angles, and tensile strength governing sliding and separation of interfaces. Furthermore, the properties of these parameters are governed by the effective stresses in the vicinity of the interface elements



and thus can soften during shaking as excess pore pressures (EPP) are generated. Table 2 presents the interface element model parameters, with frictional characteristics representing the rough interface of cast-in-place piles where failure is expected to occur within the soil neighboring the pile surface. The interface stiffnesses were selected following a sensitivity study as described by Li et al. [19].

Table 1 – Dafalias-Manzari constitutive model parameters used in the numerical simulations

Constitutive Constant	Variable	Medium Dense Sand	Dense Sand
Elasticity	G_0	125	
	ν	0.05	
Critical state	M	1.25	
	c	0.712	
	λ_c	0.019	
	e_0	0.934	
	ξ	0.70	
Yield surface	m	0.05	
Plasticity	h_0	7.05	
	c_h	0.968	
	n^b	1.1	
Dilatancy	A_0	0.704	
	n^b	3.5	
Fabric-dilatancy tensor	z_{max}	2	
	c_z	600	
Initial void ratio	e_0	0.822	0.674
Hydraulic conductivity (m/s)	K	1.1×10^{-5}	1.1×10^{-6}
Dry density (kg/m ³)	ρ	1,450	1,580

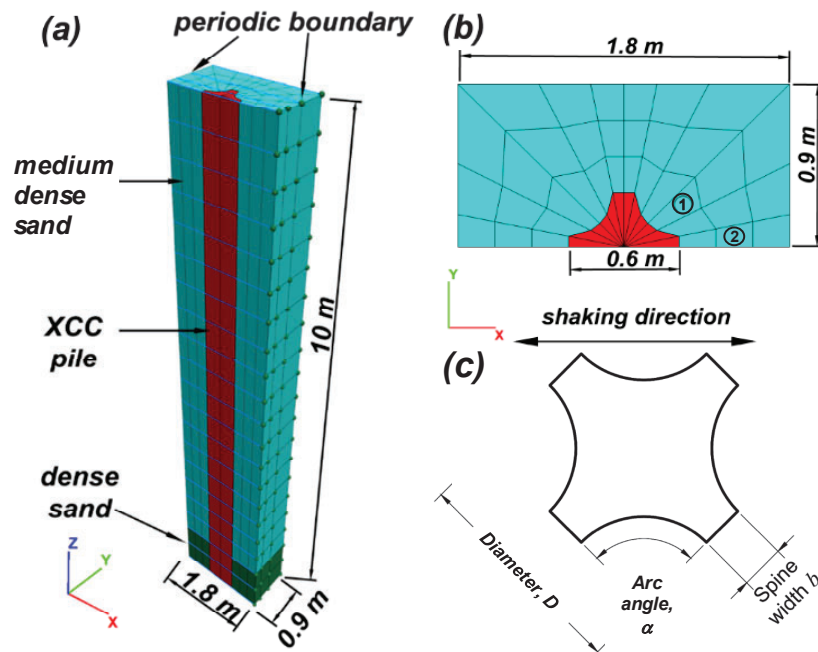


Fig. 1 – Finite difference model geometry used: (a) mesh discretization and soil layers, (b) unit cell model for XCC pile shown at 3D spacing, and (c) typical cross-section and characteristics of XCC piles.



Table 2 – Interface model parameters

Interface parameter	Medium dense sand	Dense sand
Normal stiffness	3.82×10^6 kPa/m	1.33×10^7 kPa/m
Shear stiffness	3.82×10^6 kPa/m	1.33×10^7 kPa/m
Friction angle	31°	41°

2.3 Stages of Numerical Simulation and Simulation Cases

In order to capture the appropriate stress states and boundary conditions corresponding to an infinite slope, five stages of simulation were performed prior to and during shaking. The first and second stages consist of initialization of hydrostatic pore pressures and stress states assuming linear-elastic soils under periodic boundary conditions, respectively, for the inclined unit cell. The third stage is re-equilibration by replacing the linear-elastic soil model with a Mohr-Coulomb soil model. The initial effective and shear stress state thus consisted of those of an infinite slope with:

$$\sigma_z' = (\gamma' \cos \theta) z \quad (1a)$$

$$\sigma_x' = K_o \sigma_z' \quad (1b)$$

$$\tau_{xz} = (\gamma' \sin \theta) z \quad (1c)$$

where θ = slope inclination angle, γ' = effective unit weight, z = depth below the ground surface, and K_o = at-rest geostatic earth pressure coefficient. The fourth stage replaces those soil elements to be occupied by the cast-in-place piles with the pile elements and corresponding interface elements. The constitutive model for the remaining soil elements was switched to the D-M model for the two soil layers considered and stress equilibrium re-established. Small stiffness-proportional Rayleigh damping (i.e., 0.2%) was applied to reduce high frequency noise. The fifth stage of the simulation is the dynamic analysis under various strong ground motions with fully-coupled fluid-mechanical interaction.

There are three distinct classes of numerous simulations: the first is the reference case with no piles (i.e., the unimproved, UN Case); the second case corresponds to improvement with circular piles (designated using “CA” or “CD”, depending on diameter); and the third case corresponds to improvement with XCC piles (designated using “X”). Simulations of XCC piles were performed with the spines of the pile oriented perpendicular and parallel to the slope inclination due to the superior lateral spreading mitigation performance provided by this orientation as demonstrated using shake table tests [13] and numerical simulations [19]. Table 3 summarizes the initial parametric study evaluated using the El Centro ground motion [35] scaled to 0.25g and filtered with a 5 Hz low-pass filter, with positive accelerations acting downslope. A second series of simulations, described below, were conducted to evaluate the response of the pile-improved ground with different ground motions. All simulations evaluated herein are conducted with the pile base nodes fixed against rotation for simplicity. In practice, piles driven to a competent bearing layer will exhibit a rotational stiffness smaller than infinity (fully-fixed) and larger than zero (free). The effect of pile fixity is significant as shown in an investigation considering similar soil, pile, and model conditions performed by Li et al. [19].

3. Lateral Spreading Mitigation Performance: Typical Results

One of the main objectives of this study is to demonstrate the correlation between lateral spreading performance of pile-pinned slopes and Arias Intensity, described in Section 4. This section provides a brief overview of the development of EPP under reverse cyclic loading, shear stress-shear strain hysteresis, and typical results in terms of lateral slope and pile displacements, and induced shear force and bending moment to place the results of Section 4 into an appropriate context.



Table 3 – Simulation cases evaluated using the El Centro ground motion

Case	Pile diameter, D (m)	Pile section area, A (m ²)	Pile spacing, S (m)	Area replacement ratio, a_r (%)	Slope angle
UN	/	/	/	/	0°, 4°, 7°
XS2D	0.60	0.18	1.2	12.4	4°, 7°
XS3D	0.60	0.18	1.8	5.5	4°, 7°
XS4D	0.60	0.18	2.4	3.1	4°, 7°
XS8D	0.60	0.18	4.8	0.8	4°, 7°
CAS2D*	0.48	0.18	1.2	12.4	4°, 7°
CAS3D*	0.48	0.18	1.8	5.5	4°, 7°
CAS4D*	0.48	0.18	2.4	3.1	4°, 7°
CAS8D*	0.48	0.18	4.8	0.8	4°, 7°
CDS2D	0.60	0.28	1.2	19.6	4°, 7°
CDS3D	0.60	0.28	1.8	8.7	4°, 7°
CDS4D	0.60	0.28	2.4	4.9	4°, 7°
CDS8D	0.60	0.28	4.8	1.2	4°, 7°

* The actual normalized pile spacings are $2.5D$, $3.75D$, $5D$ and $10D$, respectively; however, $2D$, $3D$, $4D$ and $8D$ are shown as they compare directly to XCC pile cases with the same center-to-center spacing and same a_r .

3.1 Generation of Excess Pore Pressure under Reverse Cyclic Loading

Figure 2 presents the EPP time histories for Cases UN, XS3D, and CAS3D for a slope inclination angle of 4° as recorded at Position 2 (Fig 1b). Whereas Case UN under level ground conditions produced a peak EPP ratio, r_u , of 0.98, the inclination angle of 4° and 7° (not shown in Fig. 2) in the unimproved slope indicated maximum $r_u = 0.70$ and 0.55 at the end of the El Centro ground motion, respectively. The reduction in EPP (relative to level ground conditions) occurs in sloping ground under the influence of an existing static shear stress, which prevents cyclic reversal (Fig. 3a). The existing static shear stress can prevent “fully-liquefied” conditions[36,37]. However, the reduced r_u does not necessarily indicate the potential for reduced lateral deformation[38]. For the pile-improved cases, the maximum r_u is larger than Case UN due to the reinforcement provided by the piling and the resulting development of shear stress reversal (Fig. 3b). In general, the EPP time histories are similar between Cases XS3D and CAS3D except for the dense sand below the interface with the medium dense sand layer ($z = 9.25$ m; Figs. 2b and 2c), where the circular pile-improved case yielded larger EPP throughout the entire ground motion.

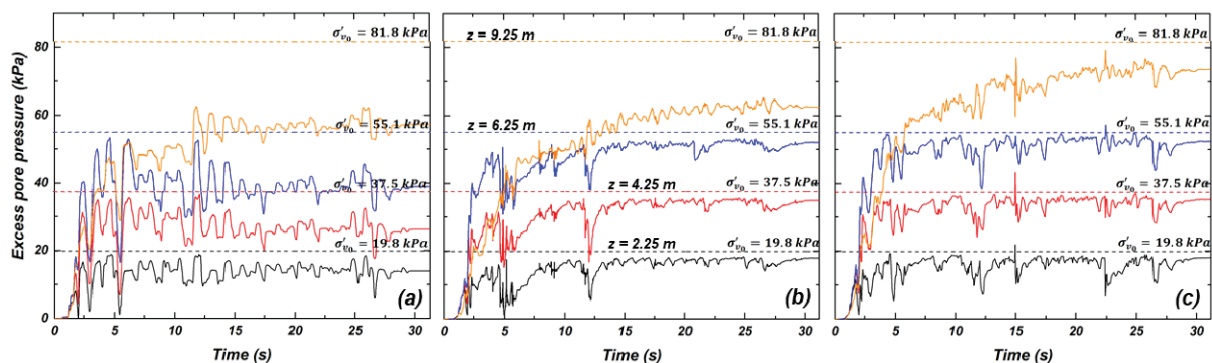


Fig. 2 – Variation of EPP time histories with depth for a slope inclination angle of 4°: (a) Case UN, (b) Case XS3D, and (c) CAS3D

3.2 Hysteretic Soil Response under Initial Static Shear Stresses

Figure 3 presents the hysteretic soil response for Cases UN and XS3D for a slope inclination angle of 4° and corresponding to Fig. 2 for comparison. Case UN indicated the significant accumulation of positive (i.e.,



downslope) shear strains with the number of cycles of loading, reaching 20% near the ground surface. Figures 3a and 3b indicates few instances of low-magnitude shear stress reversal, owing to the initial static shear stresses existing prior to shaking, thus limiting the magnitude of EPP generated. For Case XS3D, shear stress reversal occurred frequently (Figs. 3c and 3d); however, despite increased EPPs, the shear strains generally remained below 1% in the downslope (i.e. positive) direction and below 0.03% in the upslope direction. The reversal in shear stresses provides an indication of the soil-pile interaction provided by the XCC pile that serves to limit the accumulation of shear strains (and therefore lateral displacements) relative to the unimproved case. Although not shown for brevity, the hysteretic response computed for Case CAS3D was generally similar to that shown for XS3D, however notable differences in the minimum and maximum shear stresses and shear strains were observed, giving rise to differences in permanent lateral displacement and structural response of the pile, as described in detail below.

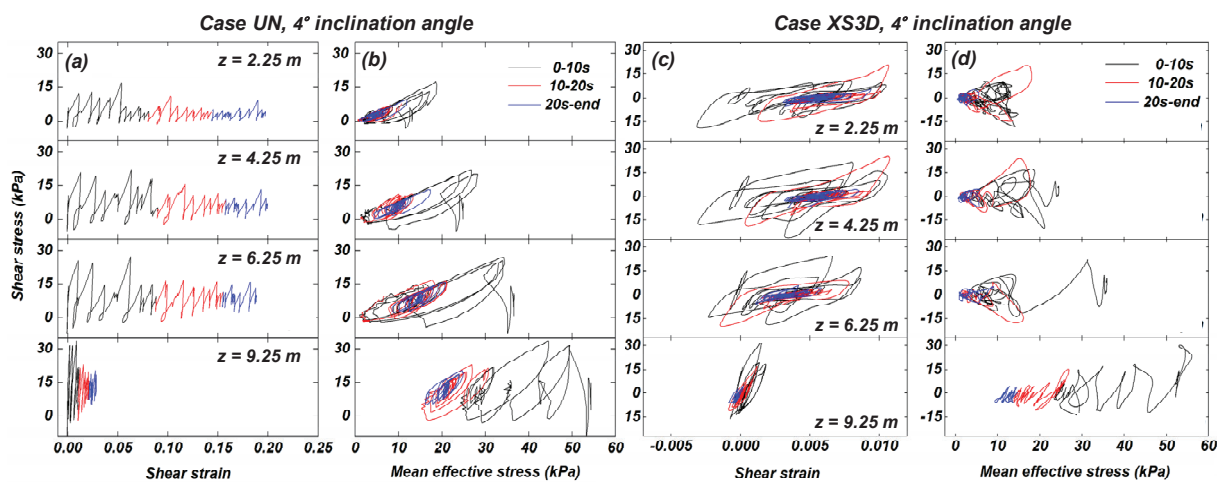


Fig. 3 – Shear stress-shear strain hysteresis and effective stress paths for (a) and (b) Case UN, and (c) and (d) Case XS3D, respectively, for an inclination angle of 4°. Note: (1) results shown for Position 1 (refer to Fig. 1b), and (2) the scale of shear strain in (a) and (c) are different.

3.3 Residual Lateral Displacement of the Soil Slope and Piles

The main objective of lateral spreading mitigation with the pile-pinning alternative is to limit the permanent or residual lateral displacements of the potentially liquefiable slope and reinforcing piles to within tolerable magnitudes. Under the El Centro ground motion, the maximum residual lateral displacement of the soil slopes for Cases UN with 4° and 7° of inclination was 1,580, and 1,380 mm, respectively. The lower magnitude of residual lateral displacement for case of a steeper inclination results from the generation of lower EPPs and fewer instances of cyclic stress reversal for this ground motion, and other ground motions may produce contrary results [19]. In comparison, the piles associated with Cases XS4D, CDS4D, CAS4D with spacing set at four diameters, produced maximum residual lateral displacements of 64, 94, 156 mm for an inclination of 4°, respectively, as shown in Fig. 4a. Thus, pile pinning at the reasonable spacing of 4D can reduce permanent residual lateral displacements by 10- to 25-fold relative to the comparable unimproved slope depending on the pile shape and diameter. For circular sections, the 20% increase in diameter (from CA to CD) and 2.5 times larger EI , resulted in a 40% reduction in displacement for the inclination of 4°. However, the use of the X-shaped cross section (which has the same section area and largest dimension as piles CA and CD, respectively) resulted in further reductions in maximum lateral pile displacement: 32% less than Case CDS4D, and 59% less than Case CAS4D. Figure 5 presents the comparison in the spatial variation of residual lateral displacements within the soil surrounding the piles following shaking for CDS4D and XS4D for the inclination of 4°; the novel cross-section of the X shape reduces the flow of softened soil around the pile and reduces the displacement magnitudes. Figure 6 presents the variation in maximum residual lateral displacement for the soil slopes and pile pinning scenarios investigated (Table 3). Naturally,



the magnitude of displacement reduction increases with a decrease in pile spacing, regardless of section geometry. Furthermore, a pile spacing of 8D is shown to reduce lateral spreading displacements of the soil slope to a third of that expected for the unimproved cases, such that even modest spacing can significantly reduce lateral displacements with the pile pinning mitigation technique. The XCC pile shape yields the smallest permanent displacements regardless of spacing owing to its novel cross section. Thus, significant material and performance efficiencies may be realized by implementing XCC piles for lateral spreading mitigation.

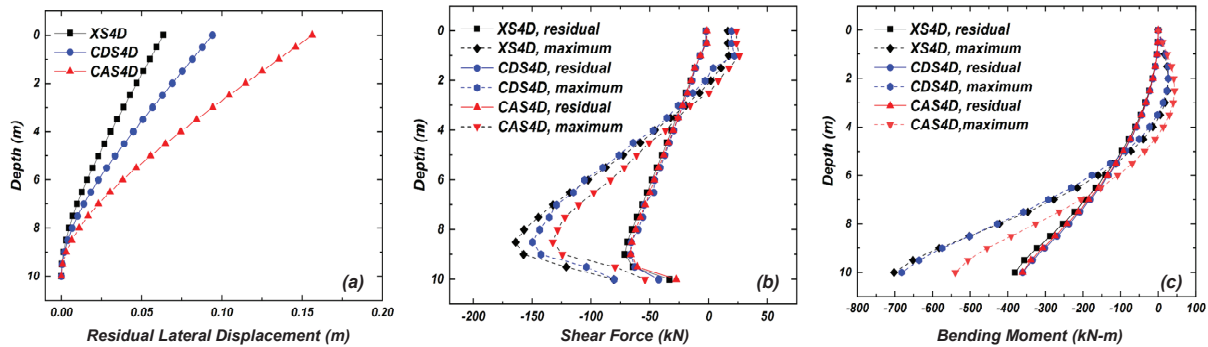


Fig. 4 – Structural response of piles with 4D spacing to lateral spreading-type loading: (a) lateral displacement of pile, (b) shear force, and (c) bending moment distributions.

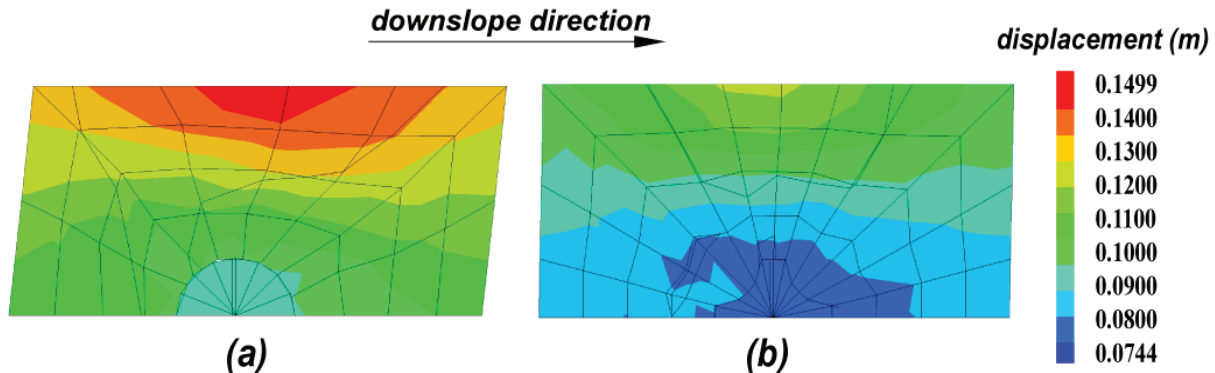


Fig. 5 – Lateral displacement (m) contours at 2.5 m depth with inclination angle of 4°: (a) Case CDS4D, with same outside diameter as (b) Case XS4D.

3.4 Structural Response of Piles to Kinematic Loading

Naturally, in order for the pile pinning technique to be deployed successfully in anticipation of design ground motions, the pile selected must provide sufficient shear and bending resistance to counteract the imposed kinematic loading. The piling was modeled using a linear-elastic constitutive model to understand the differences in the fundamental soil-pile interaction between circular and XCC piles; however, it is recognized that this simplification is unrealistic for cast-in-place piles, and that reinforcement detailing dictates the structural response. Such evaluations are underway in order to capture more realistic nonlinear moment-curvature behavior. Nonetheless, it is of interest to compare the maximum shear and bending moment between the three pile cases investigated to form preliminary opinions on their contributions to lateral spreading mitigation alternatives. Figures 4b and 4c compare the maximum and residual shear and bending moment distributions arising from the corresponding lateral displacement profiles in Fig. 4a for piles spaced at 4D. As observed by others, the maximum shear force develops near the interface between relatively soft and stiff soil layers, in this case a depth of about 9 m corresponding to the contact between the medium dense and dense sand layers. The XCC pile developed the largest maximum shear forces and bending moments, the latter significantly greater than the pile with the same section area (Case CAS4D), due



in part to the larger EI associated with the XCC pile. This stems from the reduction in soil softening due to improved soil-pile interaction and results in larger lateral soil reaction against the pile relative to the circular pile as soil flow around the XCC pile is reduced. The tendency for increased soil flow around a circular pile is partially compensated by a stiffer pile, such as that of Case CDS4D with the same largest pile dimension as that of the XCC pile, resulting in similar shear and bending moment profiles as the XCC pile. Interestingly, the residual shear forces and bending moments were not sensitive to pile shape or stiffness for the El Centro ground motion evaluated.

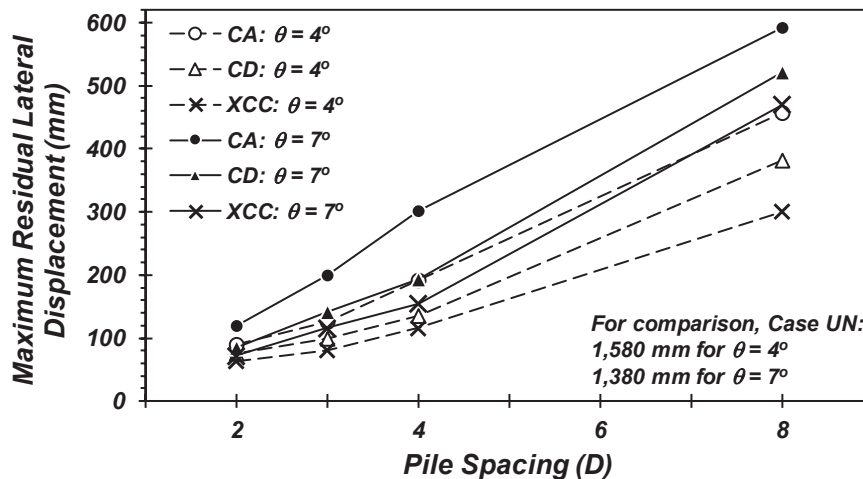


Fig. 6 – Variation of maximum residual lateral displacement of soil slope with pile spacing for XCC and circular pile-improved sloping ground

4. Assessment of Multiple Ground Motions and Correlation of Arias Intensity with Lateral Spreading Performance Metrics

The numerical simulations presented thus far corresponded a single ground motion in order to focus on the dynamic soil and soil-pile interaction giving rise to the performance of pile pinning-type lateral spreading mitigation. The effect of variable ground motion intensity, duration, and frequency content on the lateral spreading response of pile-improved ground was investigated by considering seven additional ground motions selected from the Pacific Earthquake Engineering Research (PEER) ground motion database (<https://ngawest2.berkeley.edu/site>) assembled by Jayaram et al.[39,40]. These broadband, rock site motions are seven of 40 motions whose response spectra were matched to the median and log standard deviations estimated for a M7 strike-slip earthquake with a source-to-site distance of 10 km (Table 4). The ground motions were modified by applying a 5 Hz low-pass filter and removing excessive quiet time (i.e., zero acceleration) to expedite the numerical simulations.

Table 4 – Summary of the ground motions selected from PEER database[38,39].

Ground motion	NGA Record	Year	Event	Station	Magnitude / Closest distance (km)	PGA (g)	Arias Intensity, I_A (m/s)
1	763	1989	Loma Prieta	Gilroy - Gavilan Coll.	6.9 / 10.0	0.25	0.60
2	765	1989	Loma Prieta	Gilroy Array #1	6.9 / 9.6	0.25	0.65
3	801	1989	Loma Prieta	San Jose - Santa Teresa Hills	6.9 / 14.7	0.14	0.63
4	957	1994	Northridge	Burbank - Howard Rd.	6.7 / 16.9	0.12	0.18
5	1786	1999	Hector Mine	Heart Bar State Park	7.1 / 61.2	0.06	0.10
6	1787	1999	Hector Mine	Hector	7.1 / 11.7	0.22	0.66
7	2107	2002	Denali, Alaska	Carlo	7.9 / 50.9	0.06	0.07



Among various intensity measures, Arias Intensity, I_A , has been shown to correlate to many engineering demand parameters, including liquefaction triggering[41] and seismic slope displacements[42]. Figure 7a presents an example of the displacement time histories for Cases UN, XS3D, and CDS3D to the I_A time history for NGA Record 957. A clear qualitative correlation to the evolution of lateral displacement with I_A is observed; furthermore, few differences between the response of Cases XS3D and CDS3D is observed. In general, the maximum residual lateral displacements of the soil slope for Case UN varied from 0.15 to 1.58 m (Fig. 7b), whereas the maximum, residual lateral pile displacements for Cases CDS3D and XS3D and was 0.052 m (Figs. 7c and 7d). Although slight differences in the residual pile displacement profiles exist, the responses presented in Figs. 7c and 7d clearly indicate that the shape of the XCC pile, requiring significantly less concrete volume than the circular pile that shares the same largest in-plane dimension, results in similar performance.

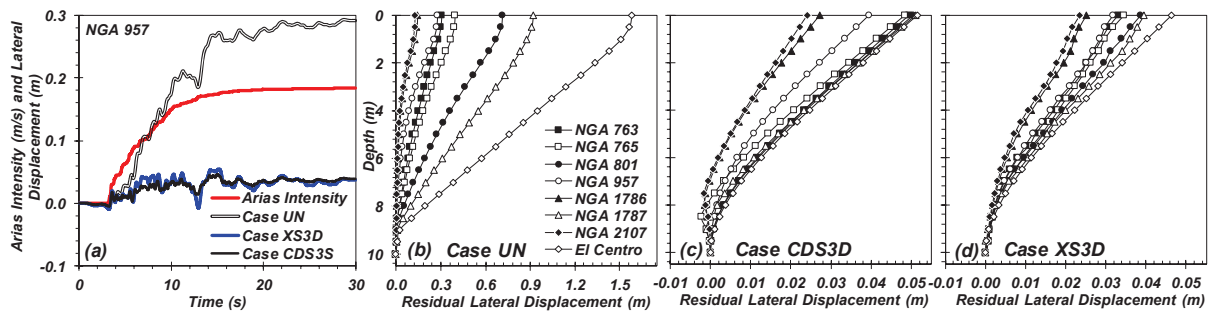


Fig. 7 – Effect of varying ground motions on the residual lateral displacements of the soil slope and piles: (a) comparison of Arias Intensity and displacement time histories, (b) soil slope displacement for Case UN, and pile displacement for (c) Case CDS3D, and (d) Case XS3D.

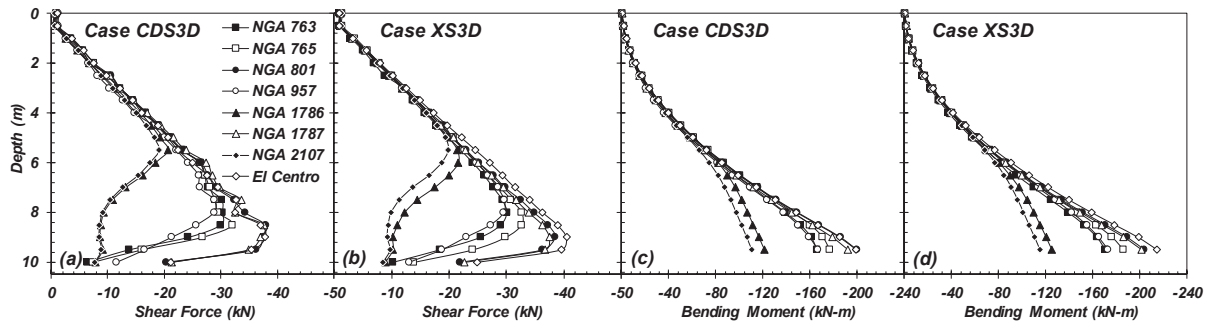


Fig. 8 – Structural response of piling to lateral spreading-type displacements: residual shear force for (a) Case CDS3D and (b) Case XS3D, and residual bending moment for (c) Case CDS3D and (d) XS3D.

The observation that the 0.6 m diameter circular pile and the XCC pile exhibit similar soil-pile interaction is further verified through the comparison of the residual shear force and bending moment profiles. Ground motions of various intensity produce varying engineering demands on the piling. As I_A increases, the locations of maximum shear force moves progressively deeper into the soil profile as more of the soil liquefies under continued shaking. NGA motions 1786 and 2107 (with $I_A \leq 0.1$ m/s) produce $r_u < 0.6$ below a depth of 6 m; the stiffness of the non-liquefied soil above the dense sand layer provides sufficient reaction to limit displacements of 25 mm or less (Figs. 7c and 7d). On the other hand, as I_A increases, the liquefied thickness of medium dense sand increases to require greater pile shear force to counteract the kinematic soil movements. The corresponding bending moment profiles exhibit a similar overall trend that a greater I_A corresponds to a larger demand on the resisting piles.

That the response of pile-improved lateral spreading-susceptible soil slope can be predicted using an evolutionary intensity measure such as the Arias Intensity of the input ground motion is of high interest to



practitioners. Although the specific characteristics (duration, intensity, frequency content) of an anticipated ground motion at a given site are difficult to predict, ground motion models (GMMs) have been improved significantly in recent years as the role of inter- and intra-site effects continue to be recognized and treated. The 3D numerical simulations conducted in this study illustrates that I_A correlates strongly to the response of pile-improved ground as demonstrated in Fig. 9, which compares I_A to the maximum residual lateral displacement, and the absolute maximum shear force and bending moment (pile-improved scenarios only) for all of the simulations. Figure 9 also illustrates the benefit of pile-pinning mitigation with regard to the reduction in lateral spreading slope displacements, and provides additional support that the shape of the XCC pile efficiently reduces soil flow due the role of its geometry in soil-pile interaction.

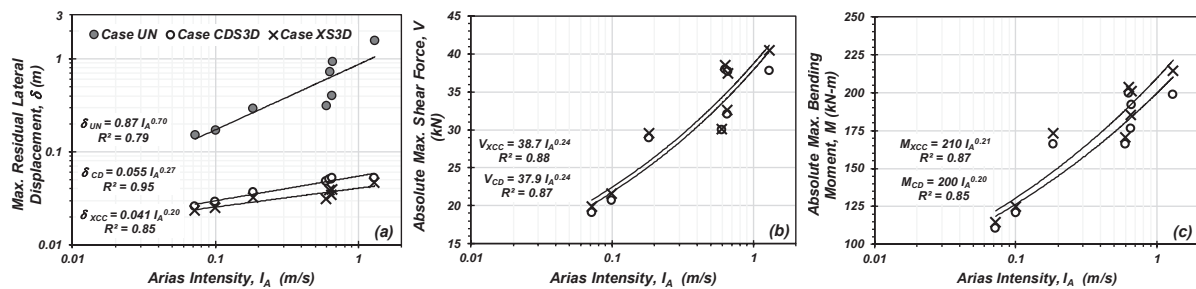


Fig. 9 – Correlation of Arias Intensity, I_A , to (a) maximum residual lateral displacement, (b) absolute maximum shear force, and (c) absolute maximum bending moment for the scenarios investigated. *Note that the XCC pile has the same maximum dimension but smaller cross-section area than circular pile CD.*

The results of the 3D numerical simulations, which capture complex hysteretic soil behavior, generation of EPP, and soil-pile interaction, indicate the beneficial effect of pile-pinning mitigation on lateral spreading type-failure. Clearly, incorporating the near-field effects of the soil-pile interaction into the assessment of seismic deformation risk can serve to justify less conservatism in design. However, these results do not include the effects of installation, intermediate rotational stiffness at the pile toe, or restraint of the pile head, all of which contribute to the seismic response of pile-improved slopes. Owing to the use of the unit cell modeling methodology, the response of piles at the boundaries of improved areas will differ from those simulated herein. Additionally, the assumption of the linear-elastic properties of the pile represents a simplification to focus on the pertinent aspects of soil-pile interaction; however, the moment-curvature response of reinforced concrete sections is nonlinear inelastic[43], and these effects should be investigated in a similar numerical setting. Finally, the simplified soil stratigraphy modeled in this study, with limited contrast in initial soil stiffness and hydraulic conductivity cannot capture the effects of layered soils, which have shown to contribute to or inhibit soil liquefaction, depending on the system response[44].

5. Concluding Remarks

This paper compares the performance of circular and X-shaped (XCC) piles in lateral spreading mitigation using numerical simulations. The XCC pile uses significantly less concrete material due to its novel cross-section intended to provide superior structural performance against the circular pile. The effect of slope inclination, pile spacing, and pile shape were investigated using the established unit cell methodology and an advanced soil constitutive model with the capability to capture the important characteristics of soil hysteresis paths and excess pore pressure generation. Comparison of the seismic response of circular piles with the same section area as that of the novel XCC pile demonstrated the geometrical advantage of the X-shaped cross-section, resulting in significantly less soil movement and pile displacement in the sloping direction. The unique geometry of the XCC pile demonstrates enhanced interaction with soils, mobilizing higher internal shear and bending moment to restrain the soil. On the other hand, a circular pile with a diameter equal to the maximum in-plane dimension of the XCC pile is required to produce similar performance, further supporting the efficiency of the method. Regardless of cross-section geometry, the Arias Intensity was strongly correlated to the lateral pile displacement, mobilized shear force, and bending moment,



indicating that this evolutionary intensity measure can serve as a reliable proxy for the assessment of anticipated lateral-spreading type performance of pile-pinning mitigations.

6. Acknowledgements

This project was supported by the Chinese National Natural Science Foundation (grant No. 51879090 and grant No.51679072), The Funds for International Cooperation and Exchange of the National Natural Science Foundation of China (Grant No. 51420105013), and the Fundamental Research Funds for the Central Universities (grant No. 2018B43214). The software usage and support from Itasca, through the IEP program, is appreciated. The authors are also grateful for the discussions with Dr. Yannis K. Chaloulos.

7. References

- [1] Brown RE. (1977): Vibroflotation compaction of cohesionless soils. *J. Geotech. Eng. Div.*, **103**(12), 1437-1451.
- [2] Kumar S. (2001): Reducing liquefaction potential using dynamic compaction and construction of stone columns. *Geotech Geol Eng*, **19**, 169–82.
- [3] Stuedlein AW, Gianella TN, Canivan G. (2016): Densification of granular soils using conventional and drained timber displacement piles. *J Geotech Geoenv. Eng*, **142**(12), 04016075.
- [4] Gianella TN, Stuedlein AW. (2017): Performance of driven displacement pile-improved ground in controlled blasting field tests. *J Geotech Geoenv. Eng*, **143**(9), 04017047.
- [5] Kitazume M. (2005): *The sand compaction pile method*. CRC Press.
- [6] Olgun CG, Martin JR. (2008): Effectiveness of jet-grout columns for mitigation of liquefaction during earthquakes. *Geotech. Eng. Disaster Mitig. Rehabil.*, Berlin, Heidelberg, 768–73.
- [7] O'Rourke TD, Goh SH. (1997): Reduction of liquefaction hazards by deep soil mixing.
- [8] Dobson T. (1997): Case histories of the vibro systems to minimize the risk of liquefaction. *Soil Improvement: A Ten Year Update*, 167–83.
- [9] Rollins KM, Anderson JKS, McCain AK, Goughnour RR. (2003): Vertical composite drains for mitigating liquefaction hazard. *Proc. Thirteen. Int. Offshore Polar Eng. Conf.*, Int. Soc. of Offshore and Polar Eng., 498–505.
- [10] Howell R, Rathje EM, Kamai R, Boulanger R. (2012): Centrifuge modeling of prefabricated vertical drains for liquefaction remediation. *J Geotech Geoenv. Eng*, **138**(3), 262–271.
- [11] Motamed R, Towhata I. (2010): Mitigation measures for pile groups behind quay walls subjected to lateral flow of liquefied soil: Shake table model tests. *Soil Dyn. Earthq. Eng.* **30**, 1043–1060.
- [12] Takahashi HA, Takahashi N, Morikawa YA, Towhata I, Takano DA. (2016): Efficacy of pile-type improvement against lateral flow of liquefied ground. *Geotechnique*, **66**(8), 617–626.
- [13] Li W, Chen Y, Stuedlein AW, Liu H, Zhang X, Yang Y. (2018): Performance of X-shaped and circular pile-improved ground subject to liquefaction-induced lateral spreading. *Soil Dyn. Earthq. Eng.*, **109**, 273–281.
- [14] Asgari A, Oliaei M, Bagheri M. (2013): Numerical simulation of improvement of a liquefiable soil layer using stone column and pile-pinning techniques. *Soil Dyn. Earthq. Eng.*, **51**, 77–96.
- [15] Cheng, Z, Jeremić, B. (2009): Numerical modeling and simulation of pile in liquefiable soil. *Soil Dyn. Earthq. Eng.*, **29**(11-12), (2009): 1405-1416.
- [16] Motamed R, Towhata I, Honda T, Tabata K, Abe A. (2013): Pile group response to liquefaction-induced lateral spreading: E-Defense large shake table test. *Soil Dyn. Earthq. Eng.*, **51**, 35–46.
- [17] Abdoun T, Dobry R, O'Rourke TD, Goh SH. (2003): Pile response to lateral spreads: centrifuge modeling. *J Geotech Geoenv. Eng*, **129**(10), 869–878.
- [18] Brandenberg SJ, Boulanger RW, Kutter BL, Chang D. (2005): Behavior of pile foundations in laterally spreading ground during centrifuge tests. *J Geotech Geoenv. Eng*, **131**(11), 1378–1391.
- [19] Li, W, Stuedlein, AW, Chen, Y, Liu, H, Cheng, Z (2019): Response of Pile Groups with X and Circular Cross-sections Subject to Lateral Spreading: 3D Numerical Simulations. *Soil Dyn. Earthq. Eng.*, **126**, 105774.
- [20] Liu H, Zhou H, Kong G. XCC pile installation effect in soft soil ground: A simplified analytical model. *Comput Geotech* 2014;62:268–82. doi:10.1016/j.compgeo.2014.07.007.
- [21] Zhou H, Liu H, Randolph MF, Kong G, Cao Z. (2017): Experimental and analytical study of X-section cast-in-place concrete pile installation effect. *Int. J. Phys. Model Geotech.*, **17**, 103–121.
- [22] Lv Y, Liu H, Ding X, Kong G. (2012): Field tests on bearing characteristics of x-section pile composite foundation. *J, Perform. Constr. Facil.*, **26**, 180–189.



- [23] Zhang D, Lv Y, Liu H, Wang M. (2015): An analytical solution for load transfer mechanism of XCC pile foundations. *Computers & Geotechnics*, **67**, 223–228.
- [24] Itasca Consulting Group Inc. (2016). *FLAC3D – Fast Lagrangian Analysis of Continua in Three-Dimensions*, Ver. 6.0, User's Guide Manual. Minneapolis: Itasca.
- [25] Walker R, Indraratna B. (2007): Vertical drain consolidation with overlapping smear zones. *Geotechnique*, **57**(5), 463–467.
- [26] Bong T, Stuedlein AW. (2018): Efficient methodology for probabilistic analysis of consolidation considering spatial variability. *Engineering Geology*, **237**, 53–63.
- [27] Stuedlein AW, Holtz RD. (2014): Displacement of Spread Footings on Aggregate Pier Reinforced Clay. *J Geotech Geoenv. Eng.*, **140**(1), 36–45.
- [28] Bong, T, Stuedlein, AW, Martin, J, Kim, B-Y. (2019): Bearing Capacity of Spread Footings on Aggregate Pier Reinforced Clay: Updates and Stress Concentration. *Canadian Geot. J.*, <https://doi.org/10.1139/cgj-2019-0026>
- [29] Rayamajhi D, Nguyen T V., Boulanger RW, Lu J, Elgamal A, Shao L. (2014): Numerical study of shear stress distribution for discrete columns in liquefiable soils. *J Geotech Geoenv. Eng.*, **140**(3), 04013034.
- [30] Chaloulos YK, Bouckovalas GD, Karamitros DK. (2013): Pile response in submerged lateral spreads: Common pitfalls of numerical and physical modeling techniques. *Soil Dyn. Earthq. Eng.*, **55**, 275–287.
- [31] Dafalias YF, Manzari MT. (2004). Simple plasticity sand model accounting for fabric change effects. *J Eng Mech*, **130**, 622–34.
- [32] Taiebat M, Dafalias YF. (2008). SANISAND : Simple anisotropic sand plasticity model. *Int J Numer Anal Methods Geomech*, **32**(8), 915–48
- [33] Cheng Z, Dafalias YF, Manzari MT. (2013). Application of SANISAND Dafalias-Manzari model in FLAC 3D. *Contin Distinct Elem Numer Model Geomech*, 09–03.
- [34] User-Defined Constitutive Models (UDM; n.d.). Itasca Consulting Group. <https://www.itascacg.com/software/udm-library> (accessed January 25, 2019).
- [35] Ulrich FP. (1941). The Imperial Valley Earthquakes of 1940. *Bull Seismol Soc Am*, **31**(1), 13–31.
- [36] Hyodo M, Murata H, Yasufuku N, Fujii T. (1991). Undrained cyclic shear strength and residual shear strain of saturated sand by cyclic triaxial tests. *Soils Found*, **31**(3), 60–76.
- [37] Pan K, Yang ZX. (2018). Effects of initial static shear on cyclic resistance and pore pressure generation of saturated sand. *Acta Geotech*, **13**(2), 473–87.
- [38] Chiaro G, Koseki J, Sato T. (2012). Effects of initial static shear on liquefaction and large deformation properties of loose saturated Toyoura sand in undrained cyclic torsional shear tests. *Soils Found*, **52**(3), 498–510.
- [39] Jayaram N, Lin T, Baker JW. (2011). A computationally efficient ground-motion selection algorithm for matching a target response spectrum mean and variance. *Earthq Spectra*, **27**(3), 797–815.
- [40] Baker JW, Lin T, Shahi SK, Jayaram N. (2011). New ground motion selection procedures and selected motions for the PEER transportation research program. *PEER Report, (2011/3)*, Pacific Earthquake Engineering Research Center, University of California, Berkeley, Berkeley, CA.
- [41] Kayen, RE, Mitchell, JK. (1997). Assessment of liquefaction potential during earthquakes by Arias intensity. *J. Geotech. Geoenviron. Eng.*, **123**(12), 1162–1175.
- [42] Kayen, R. (2017). Seismic displacement of gently-sloping coastal and marine sediment under multidirectional earthquake loading. *Engineering Geology*, **227**, 84–92.
- [43] Li, Q, Stuedlein, AW, and Marinucci, A. (2019). Effect of Casing and High-Strength Reinforcement on the Lateral Load Transfer Characteristics of Drilled Shaft Foundations. *J. Geotech. Geoenv. Eng.*, **145**(9), 04019056.
- [44] Cubrinovski, M, Rhodes, A, Ntritsos, N, & Van Ballegooy, S. (2019). System response of liquefiable deposits. *Soil Dynamics and Earthquake Engineering*, **124**, 212–229.